



Article

True Non-Contrast Phase versus Virtual-Non Contrast: “Lights and Shadows” of Dual Energy CT Angiography in Peripheral Arterial Disease

Chiara Floridi ^{1,2,3}, Laura Maria Cacioppa ³ , Giacomo Agliata ², Michaela Cellina ^{4,*} , Nicolo' Rossini ¹, Tommaso Valeri ¹, Martina Curzi ⁵, Alessandro Felicioli ³, Alessandra Bruno ¹, Marzia Rosati ³, Roberto Candelari ³ and Andrea Giovagnoni ^{1,2}

¹ Department of Clinical, Special and Dental Sciences, University Politecnica delle Marche, 60126 Ancona, Italy

² Division of Radiology, Department of Radiological Sciences, University Hospital “Azienda Ospedaliera Universitaria delle Marche”, 60126 Ancona, Italy

³ Division of Interventional Radiology, Department of Radiological Sciences, University Hospital “Azienda Ospedaliera Universitaria delle Marche”, 60126 Ancona, Italy

⁴ Radiology Department, ASST Fatebenefratelli Sacco, 20121 Milan, Italy

⁵ UOC Radiology, AST Fermo, Marche Region, 63900 Fermo, Italy

* Correspondence: michaela.cellina@asst-fbf-sacco.it



Citation: Floridi, C.; Cacioppa, L.M.; Agliata, G.; Cellina, M.; Rossini, N.; Valeri, T.; Curzi, M.; Felicioli, A.; Bruno, A.; Rosati, M.; et al. True Non-Contrast Phase versus Virtual-Non Contrast: “Lights and Shadows” of Dual Energy CT Angiography in Peripheral Arterial Disease. *Appl. Sci.* **2023**, *13*, 7134. <https://doi.org/10.3390/app13127134>

Academic Editor: Julio Garcia Flores

Received: 20 April 2023

Revised: 10 June 2023

Accepted: 12 June 2023

Published: 14 June 2023



Copyright: © 2023 by the authors. Licensee MDPI, Basel, Switzerland. This article is an open access article distributed under the terms and conditions of the Creative Commons Attribution (CC BY) license (<https://creativecommons.org/licenses/by/4.0/>).

Abstract: (1) Background: The value of dual-energy CT angiography (DE-CTA) in the detection of peripheral arterial disease (PAD) has been widely recognized. We aim to evaluate the diagnostic accuracy of virtual non-contrast (VNC) imaging of DE-CTA compared to true non-contrast phase (TNC). (2) Methods: Our Internal Review Board (IRB) approved prospective study enrolled 40 patients (28 men, 12 women; median age 69 y, range 41–93 y) who underwent lower extremity DE-CTA for symptomatic PAD. Mean attenuation values of TNC and VNC were obtained by placing circular regions of interest (ROI) at five levels from the aortic to the popliteal arterial lumen, reported in Hounsfield units (HU), and compared using a two-sample *t*-test. The subjective quality of VNC images was assessed by two independent radiologists with 10 and 4 years of CTA-imaging experience according to a 4-point scale and verified by the intra-class correlation coefficient (ICC). Dose Length Product (DLP) values of each DE-CTA examination were also considered. (3) Results: Except for the external iliac artery, VNC attenuation values were significantly lower than the corresponding TNC values at all levels, with a mean difference ranging from 14.1 and 8.7 HU. At qualitative analysis, VNC images were considered excellent to diagnose in 40%, good in 50%, and sufficient in 10% of cases. No cases of non-diagnostic VNC imaging were reported. Avoiding the TNC phase, a mean reduction in DLP of 54% for each DE-CTA was estimated. (4) Conclusions: TNC and VNC images showed comparable reliability and diagnostic accuracy in the detection of PAD. VNC may be considered a promising substitute for TNC from the perspectives of dose reduction and workflow optimization.

Keywords: computed tomography angiography; peripheral arterial disease; dual-energy computed tomography; digital scanned projection radiography; dual energy; image reconstructions

1. Introduction

Peripheral arterial disease (PAD) is characterized by arterial stenosis or occlusion anywhere from the aortoiliac axis to pedal arteries [1]. PAD has a high prevalence worldwide, occurring in up to 15% of the population over 70 years, and it is a prevalent cause of repeated hospitalizations and cardiovascular mortality [1–4].

After physical examination, imaging techniques such as Doppler ultrasound (DUS), computed tomography angiography (CTA), and digital subtraction angiography (DSA) are employed for PAD localization and definition [4]. DSA, historically the gold standard technique for PAD diagnosis, is nowadays limited to cases with a planned endovascular

therapeutic intervention due to its numerous limitations, such as radiation burden, contrast medium load, high costs, and access site complications [5,6]. For pure diagnostic purposes, DSA has been replaced by other non-invasive imaging techniques.

In current clinical practice, CTA, magnetic resonance angiography (MRA) and duplex sonography (DUS) are commonly employed to assess the extent and severity of PAD.

In particular, CTA of the lower extremity runoff is nowadays the preferred imaging modality [4,7] because of its large availability, its high resolution, the fast acquisition, and the suitability of multi-planar reconstructions (MPR) [5,8–10]. CTA is also highly accurate in assessing significant luminal lesions and evaluating arterial walls [8,11]. CTA principal drawbacks include the lack of hemodynamic information, the exposure to ionizing radiation, and the use of iodinated contrast agents. The occurrence of “blooming” artifacts caused by highly calcified atheromas resulting in an overestimation of stenosis severity and in false positive findings is also an important limitation [3–5,8,11–16].

Despite new generation CT scanners and protocols minimizing these issues [17], the increasing use of dual-energy computed tomography angiography (DE-CTA) in the diagnostic assessment of PAD may overcome CTA limitations. Specifically, DE-CTA improves the assessment of the vessel lumen lowering the employed contrast media volume [18].

As “dual-energy CT” refers to the use of two-photon spectra, DECT is frequently referred to as “spectral CT”. In the DECT dataset, since X-ray attenuation depends on the atomic number (Z) of a material, low- Z , and high- Z materials can be differentiated if images are acquired at both high and X-ray spectra (low to high tube voltages) [16]. This process, known as material decomposition, can be obtained by a variety of methods depending on the type of DE-CT scanner (equipped with a double detector panel, two X-ray tubes, or a two-layered single detector panel). The acquisition of two imaging datasets with two different attenuation profiles is thus allowed [5]. In contrast to single-spectrum imaging, DECT imaging is also able to differentiate materials with similar attenuation coefficients based on chemical composition and atomic number [19–25]. Constituent materials characterized by high atomic numbers, such as iodine and calcium, can be easily differentiated by DECT processes, thus permitting the development of many clinical applications [26]. The DE technique has several applications for clinical imaging and can allow the reduction of the iodine contrast medium dose, as well as the radiation dose.

First, material decomposition algorithms may be applied for precise quantification of specific materials such as iodine uptake. They may also generate iodine maps from contrast-enhanced phases, which may be useful in the characterization of many clinical entities [26].

Moreover, post-processing algorithms allow the identification and removal of the calcium content of calcified plaques, obtaining a better evaluation of the contrast-enhanced vessel lumen, similar to DSA images [6,11,27–37]. Imaging of arteries may benefit greatly from these DECT reconstructions. Moreover, the algorithms applied for subtracting iodine content from acquisitions, called virtual non-contrast (VNC), can be used to evaluate unenhanced vessels instead of true non-contrast (TNC) acquisitions [24,38]. At present, several software tools and clinical applications of DECT have been developed. VNC algorithms may be applied to DECT images to identify the iodine content of every single voxel and to remove the iodine component of the CT number to create images lacking in contrast material enhancement. This analysis is based on a three-material decomposition including iodine, soft tissue, and another material in relation with the anatomical district studied. The VNC algorithm is also able to quantify the iodine amount generating Iodine distribution maps. The selective removal of iodine content from post-contrast images, preserving calcium or other metallic devices is also performed with a good specificity. In vascular studies, this application may help to obtain a reconstruction of vessels without contrast from a post-contrast DE-CTA.

It has not been well established if the VNC is of acceptable quality to replace the TNC in arterial disease evaluation.

The purpose of our study is therefore to evaluate the diagnostic reliability of “virtual non-contrast” (VNC) images, obtained from the reprocessing of DE-CTA arterial scans acquired with third-generation scanners compared to baseline acquisition obtained without intravenous administration of iodinated contrast (TNC) in the study of PAD.

2. Materials and Methods

To evaluate the diagnostic reliability of VNC images obtained after DECT reconstructions, a suitable dataset was prepared. The data acquisition and elaboration is summarized in Figure 1 and described in detail in the following subsections.

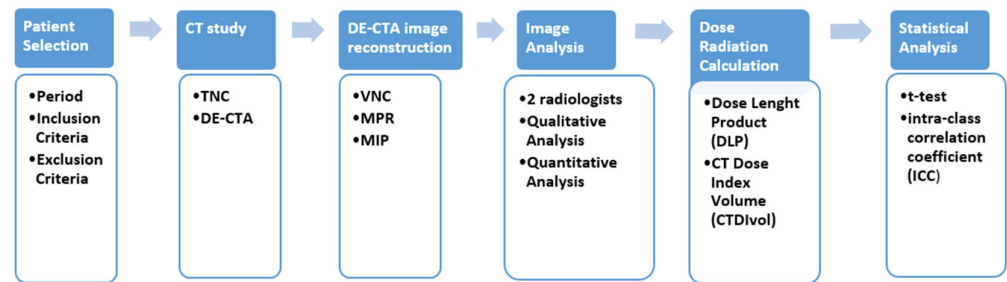


Figure 1. General diagram of methodology workflow. VNC = virtual non contrast; TNC = true non contrast; DE-CTA = dual-energy computed tomography angiography; MPR = multi-planar reformats; MIP = maximum-intensity projections.

2.1. Patient Population and Study Design

The present prospective single-center study obtained the Institutional Review Board approval of the University Politecnica delle Marche Internal Ethic Committee on 9 October 2021. Between September 2021 and May 2022, a total of 40 selected patients were enrolled. To be included, patients had to be previously submitted to a vascular evaluation for suspected chronic limb ischemia performed in the Vascular Surgery or Vascular Medicine Departments of our institution, consisting of clinical history record, physical examination, and measurement of ankle–brachial index (ABI). The clinical evaluation was also completed by a DUS examination and a laboratory test of renal function. All patients were then submitted to a CTA study of the lower limbs as required by the referring Vascular Surgeon for symptomatic PAD occurring with mild to severe claudication (Rutherford categories 1 to 3), rest pain, or non-healing minor or major ulcers (Rutherford categories 4 to 6). Patients previously submitted to stents intravascular placement, surgical revascularization, or primary amputations were excluded, as well as patients with symptoms consistent with acute limb ischemia [39].

Documented allergy to iodinated contrast medium, moderate or severe renal impairment (glomerular filtration rate < 45 mL/min), and congestive heart failure were also considered as exclusion criteria.

After the exclusion of previous allergic reactions to iodinated contrast medium, informed consent to the examination was obtained from all the participants.

Forty consecutive patients were examined for suspected PAD. Twenty-eight patients were males (median age 70 y, range, 45–85 y) and 12 patients were females (median age 69 y, range, 41–93 y). The median patient age was 69 years, ranging from 41 and 93 years. The calculated median body mass index (BMI) was 25.7 (range, 17–33.5).

Demographic and clinical characteristics of the study population were summarized in Table 1.

Table 1. Demographic and clinical characteristics of the study population.

Demographic	n (Range)
• Patients (n)	40
• Age (yrs)	69 (41–93)
• Weight (kg)	77 (53–126)
• Height (cm)	171 (158–193)
• BMI (kg/m ²)	25.7 (17–33.5)

2.2. CT Study Protocol

All studies were performed on a third-generation Dual Source Dual Energy CT scanner (Siemens Somatom Force, Siemens Healthcare, Forchheim, Germany).

All patients were positioned supine, feet first. Both feet were stabilized with adhesive tape to avoid any movements during the examination. Additionally, before the CT exam started, an 18-gauge cannula was placed into a superficial vein located in the antecubital fossa or forearm for intravenous (i.v.) contrast medium injection.

All image acquisitions were performed in the craniocaudal direction with a scan length ranging from the infrarenal abdominal aorta to the toes.

Before CT scan, patients were required to perform a deep inspiration and to hold on breath during the acquisition.

Firstly, a baseline, non-contrast, single energy acquisition was acquired with the parameters reported in Table 2.

Table 2. Single energy computed tomography (CT) and dual-energy computed tomography (DE-CT) scanning parameters.

Parameters	Single-Energy CT	DE-CT
Pitch	0.6	0.4
Slice collimation	3 mm (acquisition 192 × 0.6 mm ²)	1 mm (acquisition 192 × 0.6 mm ²)
Rotation time	0.5	0.5
Field of view (FOV)	300 mm	300 mm
Reconstruction slice thickness	3 mm	1 mm

Subsequently, DE-CTA was obtained. A 120-kVp bolus-tracking acquisition (CARE Bolus, Siemens) was used to determine scan initiation by placing a region-of-interest (ROI) in the infrarenal abdominal aorta with a trigger threshold of 300 Hounsfield units (HU) and 8-s delay. Tubes A and B were operated with 90 and 150 kVp. Image quality reference was set to 120–67 mAs. The rest of DE-CT scanning parameters were summarized in Table 1.

These scanning parameters, both of single-energy non-contrast baseline acquisition and of DE-CTA acquisition, were chosen in relation with our clinical and diagnostic experience.

For each examination, a volume of 1 mL/kg of iodinated contrast medium followed by 40 mL of saline solution at a flow rate of 4 mL/s and was intravenously administered. Automatic exposure control (CareDose 4D™, Siemens Healthcare, Forchheim, Germany) was used to adapt the tube current to variations in patient attenuation, both between different patients and within any given patient.

2.3. DE-CTA Image Reconstruction

Transverse low- and high-kVp DE-CTA imaging data were reconstructed using a medium sharp convolution kernel (Qr40). A specific dual-energy post-processing workstation with a patented algorithm (Syngo MMWP version VA 20; Siemens Healthcare, Forchheim, Germany) was used for image analysis, generating VNC images from DE-CTA images.

The algorithm is able to quantify the iodine amount of every single pixel generating an iodine distribution map. VNC images were then reconstructed to 3-mm thick axial images.

Multi-planar reformats (MPR; thickness, 1.5 mm; increment, 1.0 mm) and maximum-intensity projections (MIP; thickness, 10.0 mm; increment, 1.0 mm) in transverse, oblique coronal, and sagittal orientation were also obtained.

2.4. Image Analysis

All TNC and VNC images were reviewed by two radiologists with 12 (CF) and 9 (GA) years of experience in CTA on PACS workstations (Picture Archiving and Communication System; Centricity Radiology, GE Healthcare, Milwaukee). Only axial TNC and VNC images were assessed for qualitative and quantitative analysis.

Quantitative Analysis. The comparison of attenuation and noise between TNC and VNC images was made by drawing circular regions of interest (ROI) on both dataset images at the same level.

ROIs of approximately 0.5 cm², as large as possible for vessel caliber and avoiding vessel wall, vessel defects, plaques, and stent materials at five arterial segments, were drawn.

ROIs were positioned within the infra-renal abdominal aorta, common iliac artery, external iliac artery, femoral artery, and popliteal artery lumens.

Mean attenuation values in Hounsfield units (HU) and the corresponding standard deviation (SD) were measured as shown in Figure 2. Measurements were performed using transverse standard and MPR images and repeated three times to minimize sampling inaccuracies related to breath or movement artefacts.

Vessel	Aorta	Common iliac artery	External iliac artery	Superficial femoral artery	Popliteal artery
Arterial phase					
TNC					
VNC					

Figure 2. Arterial phase, true non-contrast (TNC) and virtual non-contrast (VNC) of dual-energy CTA run-off acquisition. In both TNC and VNC images, a circular region of interest (ROI) is placed at the level of the abdominal aorta, common iliac artery, external iliac artery, superficial femoral artery, and popliteal artery, avoiding vessel walls and plaques.

Qualitative Analysis. The two radiologists, blinded to clinical information and previous radiology reports of the examined patients, independently evaluated the quality of the CT images. The qualitative analysis was performed by using a 4-point Likert scale (4 = excellent, 3 = good, 2 = moderate but sufficient for diagnosis, and 1 = non-diagnostic) and included overall image quality, signs of residual contrast medium, possible subtracted calcifications, and stent structures.

The scores obtained with the two protocols were then compared and the inter-observer agreement was assessed, too. The specific artefacts were scored as yes/no.

2.5. Dose Radiation Calculation

Dose Length Product (DLP) and CT dose index volume (CTDIvol) values of each DE-CTA examination were also recorded from the automatically provided scan protocol to evaluate the absorbed radiation dose and its potentially harmful effects on the patient. DLP values were also standardized using gender-specific k coefficients ($K_{\text{male}} = 0.0056$, $k_{\text{female}} = 0.0068$) to obtain effective dose values (E). The effective dose values and estimated percentage of dose reduction were calculated.

2.6. Statistical Analysis

Data were analyzed using GraphPad Prism version 9.1.1 (GraphPad Software, Boston, MA, USA) statistical software. For all numerical values derived from multiple measurements, the mean value and SD were reported. The mean attenuation values of TNC and VNC images were compared using a paired measures test (*t*-test). A *p*-value < 0.05 was considered statistically significant.

The qualitative assessment was analyzed by the intra-class correlation coefficient (ICC) in the form of “Two-Way Random-Effects Model, absolute agreement, two raters/measurements”, and interpreted as follows: for values <0.4, the agreement was poor; for values between 0.4–0.59, the agreement was fair; for values between 0.6–0.79, the agreement was good; and for values between 0.8–1, the agreement was excellent.

3. Results

All DE-CTA examinations were successfully performed without any adverse events. VNC images were compared to baseline TNC scan images. No significant motion or breath artifacts were registered. Intravascular attenuation measurements were performed using ROIs as previously described and reported as HU \pm SD for TNC and VNC images. The data were subsequently compared using a test for paired measures.

At the level of the infrarenal abdominal aorta, the mean intravascular attenuation value in TNC images was 47.1 ± 6.6 HU and the corresponding value in VNC images was 33.0 ± 8.2 HU ($p < 0.00$). For common iliac artery, the mean intravascular attenuation values were 47.8 ± 8.9 HU in TNC and 34.1 ± 11.4 HU in VNC images ($p < 0.00$).

At the level of the superficial femoral artery, the mean intravascular attenuation value was 48.5 ± 9.0 HU in TNC images while the corresponding value in VNC images was 38.2 ± 10.4 HU ($p < 0.001$).

At the level of the popliteal artery, the mean intravascular attenuation values were 49.4 ± 7.8 HU in TNC and 40.7 ± 9.6 HU in VNC images ($p < 0.001$).

Finally, for the external iliac artery, the same values were 46.6 ± 9.4 HU in TNC images and 33.1 ± 6.4 HU in VNC images ($p = \text{ns}$).

The results of the attenuation comparison of TNC and VNC images at the examined levels have been summarized in Table 3.

In all the examined regions, TNC images showed significantly higher attenuation values ($p < 0.001$) than VNC images, with a mean difference of attenuation ranging from 14.1 and 8.7 HU, except for the level of the external iliac artery, where no statistically significant differences in terms of attenuation were registered ($p < 0.27$). In detail, a mean intravascular attenuation difference of 14.1 HU between TNC and VNC images at the level of the infrarenal aorta, a difference of 13.7 HU at the level of the common iliac artery, a difference of 13.5 HU at the level of the external iliac artery, a difference of 10.3 HU at the level of the superficial femoral artery, and a difference of 8.3 HU at level of popliteal artery were detected. The cumulative results of this analysis have been reported in Figure 3. Furthermore, the comparison of intravascular attenuation detected in TNC and VNC scans demonstrated less difference in HU value as the vessel caliber decreases, from the abdominal aorta to the popliteal segment, as shown in the diagram in Figure 4.

Table 3. Results of the comparison between true non-contrast (TNC) and virtual non-contrast (VNC) images in the different analyzed arterial segments: abdominal aorta, common iliac artery (AIC), external iliac artery (AIE), superficial femoral artery (AFS), popliteal artery (AP).

Anatomical Region	Contrast Phase	Mean Attenuation (HU)	Standard Deviation (DS)	<i>p</i>
Aorta	TNC	47.1	6.6	<0.000
	VNC	33.0	8.2	
AIC	TNC	47.8	8.9	<0.000
	VNC	34.1	11.4	
AIE	TNC	46.6	9.4	<0.27
	VNC	33.1	6.4	
AFS	TNC	48.5	9.0	<0.001
	VNC	38.2	10.4	
AP	TNC	49.4	7.8	<0.000
	VNC	40.7	9.6	

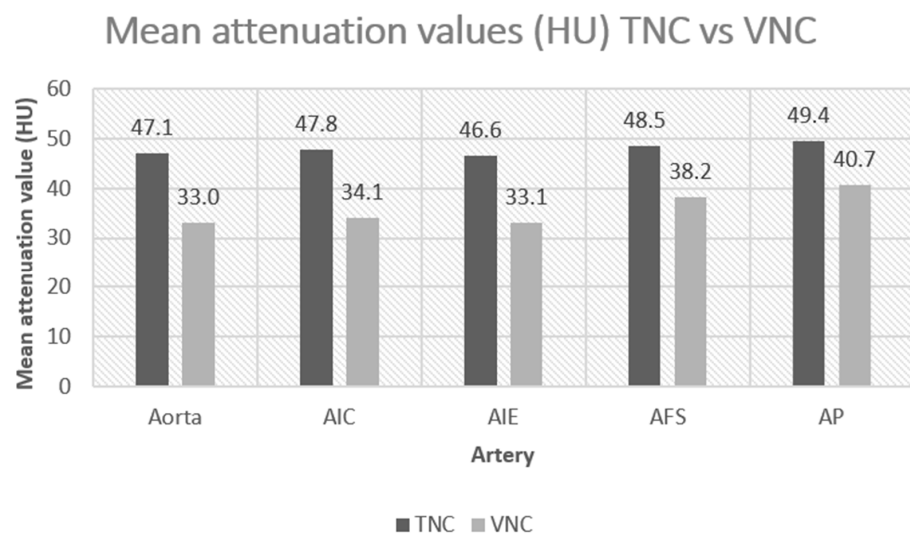


Figure 3. Bar graphs showing the comparison between mean attenuation values (HU) of true non-contrast (TNC) and virtual non-contrast (VNC) images in the different arterial segments analyzed: abdominal aorta, common iliac artery (AIC), external iliac artery (AIE), superficial femoral artery (AFS), popliteal artery (AP).

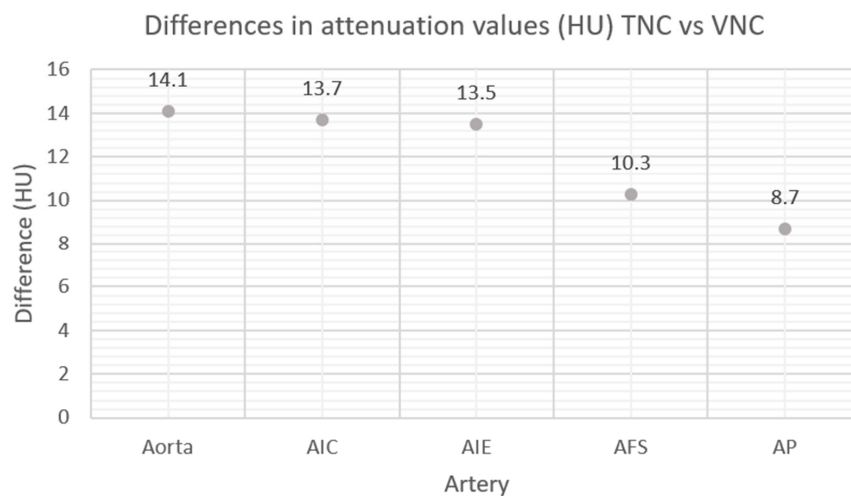


Figure 4. Differences in attenuation values (HU) between true non-contrast and virtual non-contrast images: the difference in HU value reduces as the vessel caliber decreases from the infrarenal aorta to the popliteal segment. AIC = common iliac artery; AIE = external iliac artery; AFS = superficial femoral artery; AP = popliteal artery.

Comprehensive results of the subjective qualitative analysis of VNC and TNC images performed by the two blinded observers were illustrated in Figure 5. All TNC images were rated as good in 10 (25%) cases and excellent in 30 (75%) cases (scores 3 and 4, respectively) while VNC images were rated as moderate in 4 (10%) cases, good in 20 (50%) cases, and excellent in 16 (40%) cases (scores 2, 3 and 4, respectively). All VNC images were judged sufficient for diagnosis. No cases of insufficiently diagnostic images were encountered by the two observers.

Cumulative results of qualitative analysis of VNC images

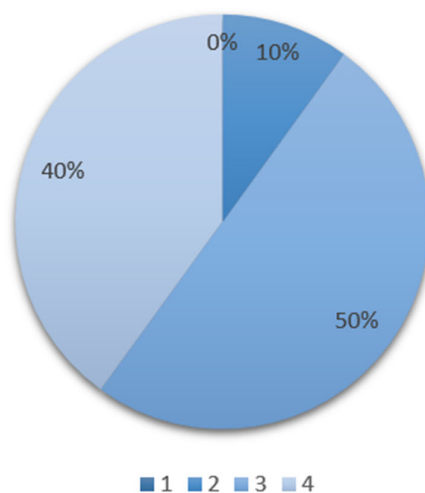


Figure 5. Cumulative results of qualitative analysis of virtual non-contrast images: 40% rated with a score of 4 (excellent); 50% with a score of 3 (good) and 10% with a score of 2 (moderate but sufficient for diagnosis). No virtual non-contrast reconstructions were considered non-diagnostic: 0% rated with a score of 1 in qualitative analysis.

The calculated ICC for the assessment of VNC images was good (0.6) while the ICC of TNC images resulted was excellent (0.9).

No cases of significant artefacts related to the permanence of iodine traces or due to the removal of stents or other devices were reported after the assessment of VNC images. Furthermore, in VNC reconstructions, highly calcified plaques were never improperly removed but, at most, were slightly attenuated.

The mean Dose Length Product (mGycm) for TNC acquisition was 546 mGycm while the mean DLP related to the DE-CTA arterial phase without the TNC acquisition was 463.5 mGycm. CT dose index volume (CTDIvol) measured values were 3.7 (2.4–9.4) for TNC acquisitions and 3.5 (1.1–6.6) for DE-CTA examinations without the TNC phase. The effective dose value of TNC acquisition was 3.25 (1.72–5.39) mSv while the effective dose value of contrast-enhanced acquisition alone was 2.76 (0.89–5.19) mSv.

The cumulative dosimetric data of TNC and arterial phases acquisitions of all DE-CTA examinations have been summarized in Table 4.

Table 4. Mean CT dose index volume (CTDIvol), mean Dose Length Product (DLP) and effective dose € values in true non-contrast and virtual non-contrast acquisitions.

Parameters	TNC	VNC
CTDI vol	3.7 (2.4–9.4)	3.5 (1.1–6.6)
DLP (mGyxcM)	546 (289–906)	463.5 (150–871)
E (mSv)	3.25 (1.72–5.39)	2.76 (0.89–5.19)

Therefore, a single DE-CTA scan with the lack of the TNC phase and completed by VNC reconstructed images may have resulted in a reduction of the administered mean effective dose.

4. Discussion

This prospective study based on 40 consecutive extremities DE-CTA scans was carried out to compare the image quality of TNC to VNC images, including attenuation and noise, as well as estimating the potential reduction in radiation dose. Based on the study results, firstly, VNC showed a good reliability in the detection of PAD in comparison to standard TNC phase; secondly, VNC reconstructions reported a high diagnostic quality at subjective analysis; and, thirdly, DE-CTA scans with the single VNC reconstructed images could result in a reduction of the administered mean effective dose.

The role of CTA in the assessment of the extent and severity of symptomatic PAD has been widely recognized by both the latest Guidelines from the American College of Cardiology/American Heart Association and the European Society of Cardiology [4,13]. Due to the recent advances in protocols and post-processing reconstructions and in lowering the amounts of radiation dose and contrast, CTA has therefore effectively replaced DSA as a first-line examination for diagnosing PAD.

As reported by previous studies, the advancement of third generation DECT and material decomposition algorithms may help in limiting blooming artifacts caused by dense calcifications and high iodine concentrations. DECT also enables a better assessment of the arterial lumen, avoiding stenosis overestimations [16]. With these assumptions, DECT imaging may be considered a valid alternative to conventional maximum intensity projection (MIP) standard reconstructions [16].

After a careful literature review, several studies were found to have attempted to account for VNC reconstructions as an alternative to standard non-contrast phases, all with controversial results [40–45]. Most of these studies were limited to the aorto-iliac attenuation values, except for one series, which has also been extended to the femoral axis [40]. Our study is one of the few to evaluate arterial lower limb vessels from the aortic axis to popliteal segments.

Since the anatomy and pathophysiology of femoropopliteal axis leads to specific challenges for both percutaneous and endovascular treatment, its non-invasive diagnosis is crucial to define the appropriate treatment strategy [2–4]. A great part of clinically significant PAD arises from femoropopliteal calcified lesions. Furthermore, endovascular treatments of this district are often challenging due to the important reactions to injuries of the thick arterial walls, which are prone to scar, proliferate, and thrombose. For these reasons, VNC reconstructions may significantly improve the evaluation of highly calcified steno-occlusive lesions of these segments [5].

Some authors reported a substantial agreement of intravascular attenuation values measured in the abdominal aorta between VNC reconstructions and TNC acquisitions [40,41]. Other studies have instead demonstrated a statistically significant difference in attenuation values at the same level, as confirmed by our series [40,43].

A greater difference in attenuation between the two CT protocols was detected in proximal vessels (aorto-iliac axis) and less pronounced in distal vessels (popliteal artery), except for the external iliac artery. This phenomenon could be explained by the different behavior of the homogeneous iodine distribution in parenchymatous tissues compared to laminar intravascular flow. The latter may lead to inaccuracies during VNC reconstructions due to blood motion artifacts. As proof of this, the greater accuracy in attenuation measurements at the level of the external iliac artery may be due to its anatomical characteristics and its lower flow [40–45].

The significantly lower attenuation values of VNC Images could be due to the very high concentration of iodine during the arterial phase. This phenomenon determines, against the expectations, an excessive iodine removal during reconstructions, and consequent lower HU-values in VNC images [45]. As previously suggested by Sauter et al. [45],

this event may be reduced by the preference for contrast media with lower iodine concentrations, with the added advantage to reduce the iodine amount in older patients and those with chronic renal impairment. This interesting hypothesis is worth verifying in future studies.

Despite these considerations, the attenuation values measured in each arterial level have differed by 15 HU or less. The data provided by the vendor report a maximum average error of 10 HU in the performance of the reconstruction algorithm, which is better set for solid parenchyma rather than arterial vessels.

In the Sauter et al. [45] and Zhang et al. series [44], differences in attenuations between VNC and TNC images lower or equal to 10 HU were considered negligible, whereas differences between 10 and 15 HU were considered acceptable [44,45]. According to those results, our attenuation differences between TNC and VNC images were 10 HU or less in 40% of cases (superficial femoral artery and popliteal artery) and 10–15 HU in 60% (abdominal aorta, common iliac artery, and external iliac artery).

Even if a modified algorithm for calcium subtraction has been recently developed [5], allowing selective removal of calcified plaques, the arterial wall calcifications of the segments were included in VNC images by our post-processing algorithm. A slight attenuation, still enabling an accurate evaluation of the arterial wall and providing an improved luminal visualization, was only featured.

The results of the subjective analysis revealed a quality rated between good and excellent in 90% of VNC images examined. No reported non-diagnostic scores, no significant invalidating artifacts, and a good degree of concordance at inter-observer evaluation were found. These results are aligned with previous studies in demonstrating how subjective evaluation of image quality has not been significantly affected by VNC reconstruction [16,40].

The present study has several important limitations. Firstly, the single-center design was with a relatively small sample size. The second limitation is the heterogeneity of the study population in terms of demographic and clinical factors. In addition, the applicability of our results is limited to a DE-CTA dataset and to this vendor-specific Virtual Unenhanced analysis algorithm. As a last important limitation, the subjective scoring biases must be considered, regardless of the double-blinded and independent evaluations.

As future perspectives, given the limited size of the study group, our primary aim lies in enlarging the patient population in terms of size and indications. In addition to cases of clinically suspected PAD submitted to this study, in which DE-CTA with VNC reconstruction may help in establishing the degree of arterial stenoses, cases of treated PAD submitted to routinely follow-up DE-CTA should be further investigated. In such cases, DE-CTA imaging may contribute significantly to improve intravascular attenuation of stented arterial segments and in reducing prosthetic artifacts. The additional advantage of lowering radiation dose when repeated CT examinations are requested, as in post-operative follow-up, is also not insignificant.

Latest advanced DE-CTA technologies, such as rapid voltage-switching and energy-sensitive detector technology, should also be considered to obtain better results in terms of imaging quality and attenuation values.

In conclusion, despite the statistically significant difference in attenuation consisting in higher values of few HU in VNC compared to TNC, our quantitative analysis demonstrated the reliability of VNC images obtained by a third generation DECT scanner in the detection of PAD. A diagnostic quality ranging from good to excellent was also achieved. The further aim of reducing dose exposure with the introduction of VNC may be considered achieved with the finding of a 54% potential reduction of mean effective dose.

VNC reconstructions provided by DE-CTA, rather than being the current optimal alternative to standard baseline images, should be considered in a variety of selected cases. Routine multiphasic follow-up, when a reduction in radiation exposure is highly recommended or an overall acquisition time reduction is desirable, in cases of inaccurate

or inconclusive non-contrast images, and to avoid unnecessary DSA exams, are some of these situations.

The use of post-processing algorithms working on remote servers such as VNC offers the additional (and not secondary) advantage of avoiding unneeded acquisitions and reducing the high amount of generated CT images sent to the picture archiving and communication system (PACS).

Nevertheless, in daily clinical practice, where time gain, dose reduction, and data storage saving are crucial, the DE-CTA protocol with VNC reconstructions may be useful for PAD detection and for an accurate treatment planning.

Author Contributions: Conceptualization, C.F. and M.C. (Martina Curzi); methodology, G.A.; software, G.A. and M.C. (Michaela Cellina); validation, L.M.C., M.C. (Michaela Cellina) and A.F.; formal analysis, N.R.; investigation, T.V.; resources, A.B.; data curation, M.R.; writing—original draft preparation, L.M.C.; writing—review and editing, L.M.C.; visualization, M.R.; supervision, C.F.; project administration, R.C.; funding acquisition, A.G. All authors have read and agreed to the published version of the manuscript.

Funding: This research received no external funding.

Institutional Review Board Statement: The retrospective study conforms to the ethics guidelines of the Declaration of Helsinki and was approved by our Internal Review Board on 9 October 2021; patients provided their consent for the examination and use of their anonymized data.

Informed Consent Statement: Informed consent was obtained from all subjects involved in the study.

Data Availability Statement: Not applicable.

Conflicts of Interest: The authors declare no conflict of interest.

References

1. Aday, A.W.; Matsushita, K. Epidemiology of Peripheral Artery Disease and Polyvascular Disease. *Circ. Res.* **2021**, *128*, 1818–1832. [[CrossRef](#)]
2. Criqui, M.H.; Matsushita, K.; Aboyans, V.; Hess, C.N.; Hicks, C.W.; Kwan, T.W.; McDermott, M.M.; Misra, S.; Ujueta, F. Lower Extremity Peripheral Artery Disease: Contemporary Epidemiology, Management Gaps, and Future Directions: A Scientific Statement from the American Heart Association. *Circulation* **2021**, *144*, e171–e191. [[CrossRef](#)]
3. Fowkes, F.G.; Rudan, D.; Rudan, I.; Aboyans, V.; Denenberg, J.O.; McDermott, M.M.; Norman, P.E.; Sampson, U.K.; Williams, L.J.; Mensah, G.A.; et al. Comparison of global estimates of prevalence and risk factors for peripheral artery disease in 2000 and 2010: A systematic review and analysis. *Lancet* **2013**, *382*, 1329–1340. [[CrossRef](#)]
4. Aboyans, V.; Ricco, J.B.; Bartelink, M.E.L.; Björck, M.; Brodmann, M.; Cohnert, T.; Collet, J.P.; Czerny, M.; De Carlo, M.; Debus, S.; et al. 2017 ESC Guidelines on the Diagnosis and Treatment of Peripheral Arterial Diseases, in collaboration with the European Society for Vascular Surgery (ESVS): Document covering atherosclerotic disease of extracranial carotid and vertebral, mesenteric, renal, upper and lower extremity arteries Endorsed by: The European Stroke Organization (ESO) The Task Force for the Diagnosis and Treatment of Peripheral Arterial Diseases of the European Society of Cardiology (ESC) and of the European Society for Vascular Surgery (ESVS). *Eur. Heart J.* **2018**, *39*, 763–816. [[CrossRef](#)] [[PubMed](#)]
5. Shwaiki, O.; Rashwan, B.; Fink, M.A.; Kirksey, L.; Gadani, S.; Karuppasamy, K.; Melzig, C.; Thompson, D.; D’Amico, G.; Rengier, F.; et al. Lower extremity CT angiography in peripheral arterial disease: From the established approach to evolving technical developments. *Int. J. Cardiovasc. Imaging* **2021**, *37*, 3101–3114. [[CrossRef](#)]
6. Yadav, V.; Khanduri, S.; Yadav, P.; Pandey, S.; Tyagi, E.; Yadav, H.; Krishnam, A.; Hamza, M. Diagnostic Accuracy of Color Doppler and Calcium Scoring versus Dual-Energy Computed Tomography Angiography in the Assessment of Peripheral Arterial Diseases of Lower Limb. *J. Clin. Imaging Sci.* **2020**, *10*, 45. [[CrossRef](#)] [[PubMed](#)]
7. Patel, M.C.; Levin, D.C.; Parker, L.; Rao, V.M. Have CT and MR angiography replaced catheter angiography in diagnosing peripheral arterial disease? *J. Am. Coll. Radiol.* **2015**, *12*, 909–914. [[CrossRef](#)]
8. Met, R.; Bipat, S.; Legemate, D.A.; Reekers, J.A.; Koelemay, M.J. Diagnostic performance of computed tomography angiography in peripheral arterial disease: A systematic review and meta-analysis. *JAMA* **2009**, *301*, 415–424. [[CrossRef](#)]
9. Napoli, A.; Anzidei, M.; Zaccagna, F.; Cavallo Marincola, B.; Zini, C.; Brachetti, G.; Cartocci, G.; Fanelli, F.; Catalano, C.; Passariello, R. Peripheral arterial occlusive disease: Diagnostic performance and effect on therapeutic management of 64-section CT angiography. *Radiology* **2011**, *261*, 976–986. [[CrossRef](#)]
10. Itoga, N.K.; Kim, T.; Sailer, A.M.; Fleischmann, D.; Mell, M.W. Lower extremity computed tomography angiography can help predict technical success of endovascular revascularization in the superficial femoral and popliteal artery. *J. Vasc. Surg.* **2017**, *66*, 835–843.e1. [[CrossRef](#)] [[PubMed](#)]

11. Meyersohn, N.M.; Walker, T.G.; Oliveira, G.R. Advances in axial imaging of peripheral vascular disease. *Curr. Cardiol. Rep.* **2015**, *17*, 87. [[CrossRef](#)] [[PubMed](#)]
12. Criqui, M.H.; Aboyans, V. Epidemiology of peripheral artery disease. *Circ. Res.* **2015**, *116*, 1509–1526. [[CrossRef](#)] [[PubMed](#)]
13. Gerhard-Herman, M.D.; Gornik, H.L.; Barrett, C.; Barshes, N.R.; Corriere, M.A.; Drachman, D.E.; Fleisher, L.A.; Fowkes, F.G.; Hamburg, N.M.; Kinlay, S.; et al. AHA/ACC Guideline on the Management of Patients with Lower Extremity Peripheral Artery Disease: Executive Summary: A Report of the American College of Cardiology/American Heart Association Task Force on Clinical Practice Guidelines. *Circulation* **2017**, *135*, e686–e725. [[CrossRef](#)] [[PubMed](#)]
14. Iezzi, R.; Santoro, M.; Marano, R.; Di Stasi, C.; Dattesi, R.; Kirchin, M.; Tinelli, G.; Snider, F.; Bonomo, L. Low-dose multidetector CT angiography in the evaluation of infrarenal aorta and peripheral arterial occlusive disease. *Radiology* **2012**, *263*, 287–298. [[CrossRef](#)]
15. Li, P.; Xu, L.; Yang, L.; Wang, R.; Hsieh, J.; Sun, Z.; Fan, Z.; Leipsic, J.A. Blooming Artifact Reduction in Coronary Artery Calcification by A New De-blooming Algorithm: Initial Study. *Sci. Rep.* **2018**, *8*, 6945. [[CrossRef](#)]
16. De Santis, D.; De Cecco, C.N.; Schoepf, U.J.; Nance, J.W.; Yamada, R.T.; Thomas, B.A.; Otani, K.; Jacobs, B.E.; Turner, D.A.; Wichmann, J.L.; et al. Modified calcium subtraction in dual-energy CT angiography of the lower extremity runoff: Impact on diagnostic accuracy for stenosis detection. *Eur. Radiol.* **2019**, *29*, 4783–4793. [[CrossRef](#)]
17. Schicchi, N.; Fogante, M.; Oliva, M.; Esposto Pirani, P.; Agliata, G.; Giuseppetti, G.M.; Giovagnoni, A. Radiation dose and image quality with new protocol in lower extremity computed tomography angiography. *Radiol. Med.* **2019**, *124*, 184–190. [[CrossRef](#)]
18. Aschof, A.J.; Catalano, C.; Kirchin, M.A.; Krix, M.; Albrecht, T. Low radiation dose in computed tomography: The role of iodine. *Br. J. Radiol.* **2017**, *90*, 20170079. [[CrossRef](#)]
19. Yang, L.; Sun, J.; Li, J.; Peng, Y. Dual-energy spectral CT imaging of pulmonary embolism with Mycoplasma pneumoniae pneumonia in children. *Radiol. Med.* **2022**, *127*, 154–161. [[CrossRef](#)]
20. Foti, G.; Mantovani, W.; Faccioli, N.; Crivellari, G.; Romano, L.; Zorzi, C.; Carbognin, G. Identification of bone marrow edema of the knee: Diagnostic accuracy of dual-energy CT in comparison with MRI. *Radiol. Med.* **2021**, *126*, 405–413. [[CrossRef](#)]
21. Foti, G.; Lombardo, F.; Guerriero, M.; Rodella, T.; Ciccio, C.; Faccioli, N.; Serra, G.; Manenti, G. Management of vertebral compression fractures: The role of dual-energy CT in clinical practice. *Radiol. Med.* **2022**, *127*, 627–636. [[CrossRef](#)]
22. Agostini, A.; Borgheresi, A.; Carotti, M.; Ottaviani, L.; Badaloni, M.; Floridi, C.; Giovagnoni, A. Third-generation iterative reconstruction on a dual-source, high-pitch, low-dose chest CT protocol with tin filter for spectral shaping at 100 kV: A study on a small series of COVID-19 patients. *Radiol. Med.* **2021**, *126*, 388–398. [[CrossRef](#)] [[PubMed](#)]
23. Tagliati, C.; Lanza, C.; Pieroni, G.; Amici, L.; Carotti, M.; Giuseppetti, G.M.; Giovagnoni, A. Ultra-low-dose chest CT in adult patients with cystic fibrosis using a third-generation dual-source CT scanner. *Radiol. Med.* **2021**, *126*, 544–552. [[CrossRef](#)] [[PubMed](#)]
24. Agostini, A.; Borgheresi, A.; Mari, A.; Floridi, C.; Bruno, F.; Carotti, M.; Schicchi, N.; Barile, A.; Maggi, S.; Giovagnoni, A. Dual-energy CT: Theoretical principles and clinical applications. *Med. Radiol.* **2019**, *124*, 1281–1295. [[CrossRef](#)] [[PubMed](#)]
25. Sanghavi, P.S.; Jankharia, B.G. Applications of dual energy CT in clinical practice: A pictorial essay. *Indian J. Radiol. Imaging* **2019**, *29*, 289–298. [[CrossRef](#)]
26. Javadi, S.; Elsherif, S.; Bhosale, P.; Jensen, C.T.; Layman, R.R.; Jacobsen, M.C.; Le, O.; Jia, S.; Parikh, R.J.; Tamm, E.P. Quantitative attenuation accuracy of virtual non-enhanced imaging compared to that of true non-enhanced imaging on dual-source dual-energy CT. *Abdom. Radiol.* **2020**, *45*, 1100–1109. [[CrossRef](#)]
27. Cicero, G.; Mazziotti, S.; Silipigni, S.; Blandino, A.; Cantisani, V.; Pergolizzi, S.; D'Angelo, T.; Stagno, A.; Maimone, S.; Squadrito, G.; et al. Dual-energy CT quantification of fractional extracellular space in cirrhotic patients: Comparison between early and delayed equilibrium phases and correlation with oesophageal varices. *Radiol. Med.* **2021**, *126*, 761–767. [[CrossRef](#)]
28. Garnett, R. A comprehensive review of dual-energy and multi-spectral computed tomography. *Clin. Imaging* **2020**, *67*, 160–169. [[CrossRef](#)]
29. Megibow, A.J.; Kambadakone, A.; Ananthakrishnan, L. Dual-Energy Computed Tomography: Image Acquisition, Processing, and Workflow. *Radiol. Clin. North Am.* **2018**, *56*, 507–520. [[CrossRef](#)]
30. Huang, S.Y.; Nelson, R.C.; Miller, M.J.; Kim, C.Y.; Lawson, J.H.; Husarik, D.B.; Boll, D.T. Assessment of vascular contrast and depiction of stenoses in abdominopelvic and lower extremity vasculature: Comparison of dual-energy MDCT with digital subtraction angiography. *Acad. Radiol.* **2012**, *19*, 1149–1157. [[CrossRef](#)]
31. Brockmann, C.; Jochum, S.; Sadick, M.; Huck, K.; Ziegler, P.; Fink, C.; Schoenberg, S.O.; Diehl, S.J. Dual-energy CT angiography in peripheral arterial occlusive disease. *Cardiovasc. Interv. Radiol.* **2009**, *32*, 630–637. [[CrossRef](#)] [[PubMed](#)]
32. Kim, J.S.; Park, S.H.; Park, S.; Hwang, J.H.; Kim, J.H.; Pak, S.Y.; Lee, K.; Schmidt, B. Imaging Findings of Peripheral Arterial Disease on Lower-Extremity CT Angiography Using a Virtual Monoenergetic Imaging Algorithm. *J. Korean Soc. Radiol.* **2022**, *83*, 1032–1045. [[CrossRef](#)]
33. Kau, T.; Eicher, W.; Reiterer, C.; Niedermayer, M.; Rabitsch, E.; Senft, B.; Hausegger, K.A. Dual-energy CT angiography in peripheral arterial occlusive disease—accuracy of maximum intensity projections in clinical routine and subgroup analysis. *Eur. Radiol.* **2011**, *21*, 1677–1686. [[CrossRef](#)] [[PubMed](#)]
34. Klink, T.; Wilhelm, T.; Roth, C.; Heverhagen, J.T. Dual-Energy CTA in Patients with Symptomatic Peripheral Arterial Occlusive Disease: Study of Diagnostic Accuracy and Impeding Factors. *Rofo* **2017**, *189*, 441–452. [[CrossRef](#)]

35. Koo, B.J.; Won, J.H.; Choi, H.C.; Na, J.B.; Kim, J.E.; Park, M.J.; Jo, S.H.; Park, H.O.; Lee, C.E.; Kim, M.J.; et al. Automatic Plaque Removal Using Dual-Energy Computed Tomography Angiography: Diagnostic Accuracy and Utility in Patients with Peripheral Artery Disease. *Medicina* **2022**, *58*, 1435. [[CrossRef](#)]
36. Almutairi, A.; Sun, Z.; Poovathumkadavi, A.; Assar, T. Dual Energy CT Angiography of Peripheral Arterial Disease: Feasibility of Using Lower Contrast Medium Volume. *PLoS ONE* **2015**, *10*, e0139275. [[CrossRef](#)]
37. Tanaka, R.; Yoshioka, K.; Takagi, H.; Schuijf, J.D.; Arakita, K. Novel developments in non-invasive imaging of peripheral arterial disease with CT: Experience with state-of-the-art, ultra-high-resolution CT and subtraction imaging. *Clin. Radiol.* **2019**, *74*, 51–58. [[CrossRef](#)]
38. Cicero, G.; Ascenti, G.; Albrecht, M.H.; Blandino, A.; Cavallaro, M.; D'Angelo, T.; Carerj, M.L.; Vogl, T.J.; Mazziotti, S. Extra-abdominal dual-energy CT applications: A comprehensive overview. *Radiol. Med.* **2020**, *125*, 384–397. [[CrossRef](#)]
39. Björck, M.; Earnshaw, J.J.; Acosta, S.; Bastos Gonçalves, F.; Cochennec, F.; Debus, E.S.; Hinchliffe, R.; Jongkind, V.; Koelemay, M.J.W.; Menyhei, G.; et al. Editor's Choice—European Society for Vascular Surgery (ESVS) 2020 Clinical Practice Guidelines on the Management of Acute Limb Ischaemia. *Eur. J. Vasc. Endovasc. Surg.* **2020**, *59*, 173–218. [[CrossRef](#)]
40. Lee, M.H.; Park, H.J.; Kim, J.N.; Kim, M.S.; Hong, S.W.; Park, J.H.; Kang, C.H. Virtual non-contrast images from dual-energy CT angiography of the abdominal aorta and femoral arteries: Comparison with true non-contrast CT images. *Br. J. Radiol.* **2022**, *95*, 20220378. [[CrossRef](#)] [[PubMed](#)]
41. Sommer, C.M.; Schwarzwaelder, C.B.; Stiller, W.; Schindera, S.T.; Stampfl, U.; Bellemann, N.; Holzschuh, M.; Schmidt, J.; Weitz, J.; Grenacher, L.; et al. Iodine removal in intravenous dual-energy CT-cholangiography: Is virtual non-enhanced imaging effective to replace true non-enhanced imaging? *Eur. J. Radiol.* **2012**, *81*, 692–699. [[CrossRef](#)]
42. Toepker, M.; Moritz, T.; Krauss, B.; Weber, M.; Euller, G.; Mang, T.; Wolf, F.; Herold, C.J.; Ringl, H. Virtual non-contrast in second-generation, dual-energy computed tomography: Reliability of attenuation values. *Eur. J. Radiol.* **2012**, *81*, e398–e405. [[CrossRef](#)] [[PubMed](#)]
43. Lehti, L.; Söderberg, M.; Höglund, P.; Nyman, U.; Gottsäter, A.; Wassélius, J. Reliability of virtual non-contrast computed tomography angiography: Comparing it with the real deal. *Acta Radiol. Open* **2018**, *7*, 205846011879011. [[CrossRef](#)] [[PubMed](#)]
44. Zhang, L.J.; Peng, J.; Wu, S.Y.; Wang, Z.J.; Wu, X.S.; Zhou, C.S.; Ji, X.M.; Lu, G.M. Liver virtual non-enhanced CT with dual-source, dual-energy CT: A preliminary study. *Eur. Radiol.* **2010**, *20*, 2257–2264. [[CrossRef](#)] [[PubMed](#)]
45. Sauter, A.P.; Muenzel, D.; Dangelmaier, J.; Braren, R.; Pfeiffer, F.; Rummeny, E.J.; Noël, P.B.; Fingerle, A.A. Dual-layer spectral computed tomography: Virtual non-contrast in comparison to true non-contrast images. *Eur. J. Radiol.* **2018**, *104*, 108–114. [[CrossRef](#)]

Disclaimer/Publisher's Note: The statements, opinions and data contained in all publications are solely those of the individual author(s) and contributor(s) and not of MDPI and/or the editor(s). MDPI and/or the editor(s) disclaim responsibility for any injury to people or property resulting from any ideas, methods, instructions or products referred to in the content.